THE COMPANY OF
Biologists

RESEARCH ARTICLE

Head movements and the optic flow generated during the learning flights of bumblebees

Olena Riabinina[1,*], Natalie Hempel de Ibarra[2], Andrew Philippides[1] and Thomas S. Collett[3,‡]

ABSTRACT

Insects inform themselves about the 3D structure of their surroundings through motion parallax. During flight, they often simplify this task by minimising rotational image movement. Coordinated head and body movements generate rapid shifts of gaze separated by periods of almost zero rotational movement, during which the distance of objects from the insect can be estimated through pure translational optic flow. This saccadic strategy is less appropriate for assessing the distance between objects. Bees and wasps face this problem when learning the position of their nest-hole relative to objects close to it. They acquire the necessary information during specialised flights performed on leaving the nest. Here, we show that the bumblebee's saccadic strategy differs from other reported cases. In the fixations between saccades, a bumblebee's head continues to turn slowly, generating rotational flow. At specific points in learning flights these imperfect fixations generate a form of 'pivoting parallax', which is centred on the nest and enhances the visibility of features near the nest. Bumblebees may thus utilize an alternative form of motion parallax to that delivered by the standard 'saccade and fixate' strategy in which residual rotational flow plays a role in assessing the distances of objects from a focal point of interest.

KEY WORDS: Insect navigation, Pivoting parallax, Visual learning, Saccades, Active vision, Motion parallax

INTRODUCTION

Bees and wasps leaving their nest for the first time are able to relocate it on their return (Capaldi and Dyer, 1999; Tinbergen, 1932). They acquire the necessary visual information during elaborate flight manoeuvres that are known as learning flights, which these insects perform on their first few departures from the nest (Lehrer, 1993; Opfinger, 1931; Vollbehr, 1975; Wagner, 1907; Zeil, 1993a). The wasp *Cerceris* (Zeil, 1993b), honeybees (Cheng et al., 1987; Dittmar et al., 2011; Lehrer and Collett, 1994) and ground-nesting bees (Brünnert et al., 1994) seem to learn the distance of visual features from the nest or a feeding site through motion parallax. We have made high-speed video recordings of the head and body movements of the bumblebee, *Bombus terrestris* L., during phases of its learning flights when the bees are close to the nest. Analysis of the videos reveals the movement strategies through which these bees can acquire information about the distances between the nest-hole and small, nearby visual features.

Bombus terrestris nests in holes in the ground and the entrance to the nest may be obscured by vegetation, so that the exact position of the nest is only known through the arrangement of nearby visual landmarks. To learn the position of the nest in relation to such cues, bumblebees spend many seconds looping close to the ground in flight manoeuvres that are centred on the position of the nest-hole and extend only tens of centimetres from it (Philippides et al., 2013). The loops (e.g. Fig. 1A) are a major structural component of bumblebee learning flights and it is likely that cues to the position of the nest are learnt during these loops (Collett et al., 2013; Philippides et al., 2013). The bees then gradually fly higher and their loops expand until they cover many metres (Osborne et al., 2013). During this expansion, bumblebees may learn the larger, more distant visual features, which can guide the bees' return to the neighbourhood of the nest, as shown in honeybees (Becker, 1958; Capaldi and Dyer, 1999).

In addition to generating body movements appropriate for acquiring visual information, many insects refine the visual feedback generated during their locomotion by moving their head, and thus eyes, relative to the body. Several insects are known to employ a 'saccade and fixate' strategy during flight or walking (Bender and Dickinson, 2006; Blaj and van Hateren, 2004; Boeddeker et al., 2010; Land, 1973; Ribak et al., 2009; Schilstra and van Hateren, 1998; Schilstra and van Hateren, 1999; van Hateren and Schilstra, 1999), in which high speed turns in the yaw plane (saccades) are separated by periods of low rotational speed (fixations). The coordinated head and body movements that underlie this strategy have been analysed most fully in blowflies (Schilstra and van Hateren, 1998; Schilstra and van Hateren, 1999; van Hateren and Schilstra, 1999). The angular speed of the fly's head in space follows an almost rectangular profile with close to zero rotational speed between saccades and a high rotational speed during saccades. Minimising rotational flow in fixations both reduces blur (Land, 1997), so enhancing object detection, and may simplify the estimation of the distance of objects from the insect through translational parallax (Collett, 1978; Sobel, 1990; Wallace, 1959). Saccadic turns with coordinated head and body movements also occur during learning flights in *Cerceris* (Zeil et al., 2007) and in honeybees (Boeddeker et al., 2010). Insects may extract information about the position and distance of visual features relative to the insect during these fixations, when retinal image motion is mostly a consequence of the insect's translation.

Translational parallax gives information about distance relative to the observer – the faster the image of a feature moves, the closer the feature is. If an insect monitors distance through translational parallax, it can best assess the distances of objects from the nest by acquiring parallax information at the nest entrance. An alternative form of motion parallax termed 'pivoting parallax' (Voss and Zeil, 1998) can give information about the distance between the nest and

[1]Centre for Computational Neuroscience and Robotics, Department of Informatics, University of Sussex, Brighton BN1 9QJ, UK. [2]Psychology, College of Life and Environmental Sciences, University of Exeter, Exeter EX4 4QG, UK. [3]School of Life Sciences, University of Sussex, Brighton BN1 9QG, UK.
*Present address: Solomon H. Snyder Department of Neuroscience, Center for Sensory Biology, The Johns Hopkins University School of Medicine, Baltimore, MD 21205, USA.
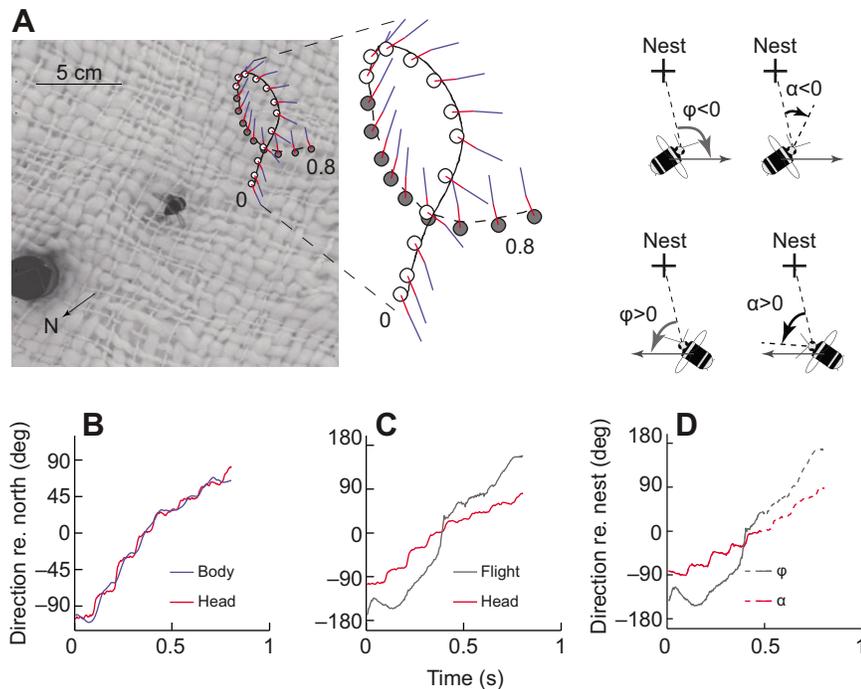
‡Author for correspondence (t.s.collett@sussex.ac.uk)

Fig. 1. The changing direction of flight and the saccadic turns of head and body during a loop. (A) A bee's flight path during a loop (0 to 0.8 s). The bee's head position is shown every 40 ms by open circles, which indicate turning towards the nest, or by filled circles, which indicate turning away from the nest. Lines indicate orientation of head (red) and body (blue). The nest-hole is in the middle of the frame, underneath the bumblebee. The loop is enlarged to the right to illustrate differences in head and body orientations. Insets define φ (the direction of flight relative to the nest), α (the orientation of the head relative to the nest) and their sign; + indicates the nest-hole. (B) Plots of body and head orientation every 4 ms in a horizontal plane. (C) Plots of flight direction and head orientation in compass coordinates. (D) Flight direction (φ) and head orientation (α) relative to the nest. The solid section of the plot marks turning towards the nest; the dashed section marks turning away from the nest.

nearby features when the bee is at a variety of positions. In this case, an insect keeps the nest stationary on the retina while moving around the nest. The apparent displacement of a feature in the surroundings increases with the feature's distance from the nest. Features close to the nest will be clearly visible as they are almost stationary and contrast with the blurred moving images of more distant features. As long as the nest area remains the centre of rotation, the movements can expand in scale and the observer will continue to obtain nest-based distance information.

Learning flights recorded with low temporal and spatial resolution indicated that *Cerceris* perform pivoting parallax (Zeil, 1993a), but later high speed recordings of the head movements of *Cerceris* and honeybees revealed a 'perfect' saccade and fixate strategy (Boeddeker et al., 2010; Zeil et al., 2007), suggesting instead that these insects gain distance information through translational parallax. The data presented below show that bumblebees have a saccade and fixate strategy that leaves a substantial residue of rotational flow. This rotational flow may help implement a form of pivoting parallax during phases of learning flights that are appropriate for acquiring knowledge about visual features near the nest.

RESULTS

We start by describing the unusual saccade and fixate strategy that we find in bumblebee learning flights recorded at high temporal and spatial resolution. To emphasise the differences from other studies, we add the prefix 'pseudo-' to 'fixation'. Next, we show that the combined effect of body and head movements during pseudo-fixations is to produce pivoting parallax limited to a specific phase of the loops of learning flights, and that the same optic flow pattern is seen in flights recorded at low resolution over a larger area.

The Appendix contains an analysis of recordings that were made to assess the extent to which measurements of yaw during fixations may be contaminated by roll. We conclude that roll and yaw are not closely correlated and that roll adds noise rather than systematically biasing yaw estimates.

Saccades and pseudo-fixations during learning flights

In bumblebees, as in the wasp *Cerceris* and the honeybee, head movements relative to the body introduce a marked saccadic structure to the bumblebee's changing direction of gaze during learning flights. The saccadic changes in head orientation and the more gradual changes of body orientation during a bumblebee learning flight are seen in the different rotational speeds of the head and body (Fig. 1B).

The median absolute speed of head rotation during 627 extracted clockwise (CW) and counter-clockwise (CCW) saccades is 657 deg s^{-1} [inter-quartile range (IQR): 543–780 deg s^{-1}, Fig. 2A]. The speed of head saccades increases from about 400 deg s^{-1} to 1000 deg s^{-1} as their amplitude increases from about 7 to 35 deg (supplementary material Fig. S1A). Body speeds over the same time period are significantly lower ($P<0.0001$), with a median speed of 344 deg s^{-1} (IQR: 213–499 deg s^{-1}, $N=627$, Fig. 2A). Head and body speeds during pseudo-fixations also differ significantly ($P<0.0001$). Median absolute head speed is 36 deg s^{-1} (IQR: 17–64 deg s^{-1}, $N=395$), significantly lower than the median absolute body speed of 104 deg s^{-1} (IQR: 44–204 deg s^{-1}, $N=395$).

Pseudo-fixations begin (Fig. 2B, 'start' panels) with the head abruptly reducing speed, but not quite to zero. The body slows down more gradually and slightly later. Pseudo-fixations end and saccades start (Fig. 2B, 'end' panels) with the head and body accelerating together, but with the head turning at a much higher speed. The residual head movement during pseudo-fixations is mostly in the same direction as in the flanking saccades (Fig. 1B,C, Fig. 2). If pseudo-fixations are categorised according to whether the neighbouring saccades are CW (negative direction) or CCW (positive direction), head rotation is in the same direction as in the flanking saccades in 69% of CW and 74% of CCW pseudo-fixations. Head speeds during CW and CCW pseudo-fixations differ significantly from each other (CCW: median: 31 deg s^{-1}, IQR: −3 to 62 deg s^{-1}, $N=212$; CW: median: −25 deg s^{-1}, IQR: −60 to 14 deg s^{-1}, $N=183$, $P<0.0001$) and from zero (CCW: $P<0.0001$, CW: $P<0.0001$).
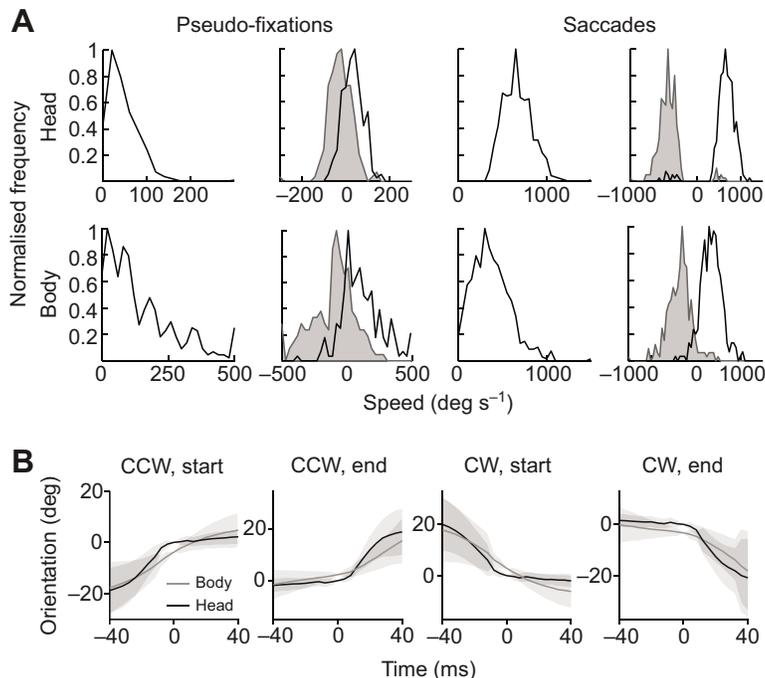
Fig. 2. Head and body speed during saccades and pseudo-fixations. (A) Angular speed of head and body during pseudo-fixations (columns 1 and 2) and saccades (columns 3 and 4). Columns 1 and 3 give distributions of absolute angular speeds. Columns 2 and 4 show distributions of angular speeds of pseudo-fixations and saccades sorted according to the predominant clockwise (CW; grey lines, shaded) or counter-clockwise (CCW; black lines) direction of rotation of the flight segments in which they occur (e.g. supplementary material Fig. S1Cii). Top row: head speed; bottom row: body speed. (B) Time plots of the mean orientation of the head and body at transitions between saccades and pseudo-fixations. First and third panels: start of pseudo-fixation. Second and fourth panels: end of pseudo-fixation. Orientation and times of individual plots are centred on (0,0). Shaded areas mark ±1 s.d. from the mean.

Pseudo-fixations during manoeuvres of learning flight

Residual head movements during pseudo-fixations may in part be the outcome of a control system that reduces head rotation by minimising optic flow. Whether or not that is so, the bee's flight pattern combined with residual head movements introduces a potential for extracting information from pivoting parallax movements during specific phases of the loops of learning flights (Collett et al., 2013; Philippides et al., 2013). During a loop, bees fly and turn towards the nest-hole, then face it and fly towards it, before turning and flying away (e.g. Fig. 1A). Below (see 'Signs of pivoting parallax detected in low speed recordings'), we present data from low resolution recordings, in which head movements are not resolved, illustrating that pivoting parallax could occur during the phase of loops in which bees turn towards the nest.

Fig. 3 shows the same pattern for high resolution recordings. Whole loops are not often captured at high spatial resolution and we mostly analysed loop fragments. We therefore classified pseudo-fixations according to whether the nest entrance slips forward (turns towards the nest) or backward (turns away from the nest) across the retina during flanking saccades, as given by a decrease or an increase in the absolute magnitude of the angle α, respectively (Fig. 3). α is equivalently the orientation of the bees' head relative to the nest, or the retinal position of the image of the nest.

In Fig. 3A,B, the rotational speeds of the head and body are plotted against α for turns towards and turns away from the nest. The average speeds associated with turns towards the nest (left column) cluster in the top left and bottom right quadrants, indicating that during these pseudo-fixations both head and body continue to rotate in the direction of the nest. The median absolute rotational speed of the head is 46 deg s^{-1} (IQR: 22–78 deg s^{-1}, N=222). The body turns at a significantly higher median speed (126 deg s^{-1}, IQR: 65–252 deg s^{-1}, N=222, P<0.0001).

No such pattern of head and body movements occurs during pseudo-fixations away from the nest, in which the nest moves backwards over the retina (Fig. 3A,B, right column). Head and body rotate more slowly and in both directions so that mean head and body speeds are roughly 0 deg s^{-1} over the whole range of body

orientations relative to the nest (Pearson's linear correlation, head: ρ=–0.03, P=0.72; body: ρ=0.08, P=0.3). Absolute rotational speed of the body in space is again higher than absolute head speed (head speed: 30 deg s^{-1}, IQR: 14–48 deg s^{-1}, N=173; body speed: 81 deg s^{-1}, IQR: 30–157 deg s^{-1}, N=173), but the two speeds are significantly lower than their counterparts during pseudo-fixations towards the nest (head: P<0.0001, body: P<0.0001).

A parallel but smaller difference in the rotational speed of the head occurs during saccades (supplementary material Fig. S1B). The median speed of head rotation is 682 deg s^{-1} (IQR: 554–806 deg s^{-1}) in saccades towards the nest, and slightly but significantly (P<0.001) slower in saccades away from the nest (median speed of head rotation: 631 deg s^{-1}, IQR: 536–718 deg s^{-1}).

The differences in head rotation between turns towards or away from the nest are primarily a result of differences in body rotation. Head movement with respect to the body is similar across the two turn directions, as seen in the linear central portion of the plot of mean head speed against mean body speed during each pseudo-fixation (Fig. 3C). As in other insects, the head counter-rotates on the body to compensate for body rotation, but, unlike other reported cases, compensation is partial. Between −200 and 200 deg s^{-1}, regression coefficients for turns towards and away from the nest are significantly less than −1 (towards the nest: −0.73±0.025: away: −0.75±0.025, Student's t-test P<0.0001), but do not differ significantly from each other (ANOVA, d.f.=1, F=0.97, P=0.33).

Patterns of optic flow during pseudo-fixations

Rotational and translational optic flow combine in determining the motion of features across the retina. Rotational optic flow dominates translational flow during saccades, but the two components are more closely balanced during pseudo-fixations and may either add to or oppose each other. The magnitude of the translational component of optic flow generated by a feature drops with its distance from the bee, but the rotational component is independent of distance. The data for regions near the nest in Fig. 3D show that in turns towards the nest the two components of optic flow tend on average to cancel each other out, whereas in turns away from the nest the two
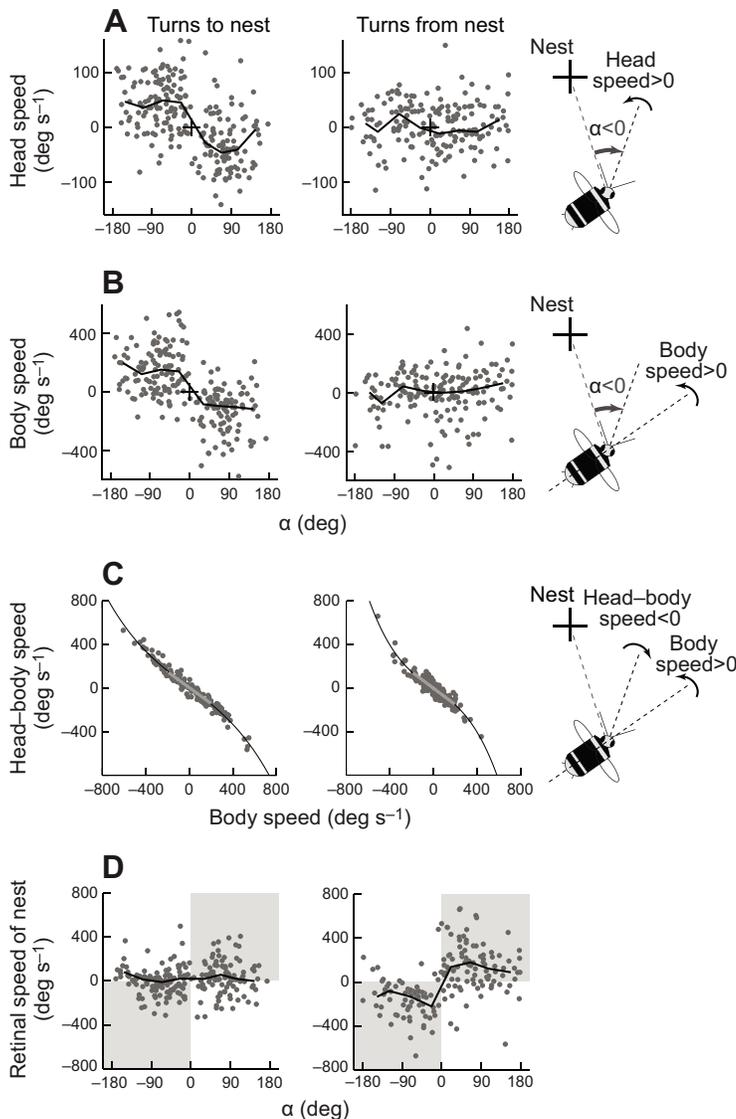
Fig. 3. Head and body movements during pseudo-fixations when bees turn towards (left column) or away from (right column) the nest. (A) Head speed in space plotted against the orientation of the head relative to the nest (α). Black solid lines show average speed calculated over 30 deg wide bins of head orientation. The + sign on the plot indicates the (0,0) point of the coordinate system. Each grey data point represents speed and orientation, averaged over one pseudo-fixation. (B) Similar plot for body speed. (C) Speed of head relative to body. The data are well fitted by the following cubic functions: turns towards nest $y=-6.4\times10^{-7}x^3-2.8\times10^{-5}x^2-0.74x+6.7$; turns from nest: $y=-2\times10^{-6}x^3-1.1\times10^{-5}x^2-0.68x-1.9$, but the central portion of the plot is more linear (thick grey lines show linear fit). (D) Retinal speed of nest during pseudo-fixations, with retinal speed defined by rate of change of α. Solid lines show averages calculated over 30 deg bins of alpha.

components reinforce each other. Consequently, in turns towards the nest, features around it can gain visibility by appearing almost stationary against a background of motion in the opposite direction.

A significant difference ($P<0.0001$) between the image speeds of the nest during turns towards and away from the nest persists if we take the absolute image speed of the nest and average it over the whole range of head orientations. The absolute value of the image speed of the nest during turns towards the nest is 71 deg s^{-1} (IQR: 31–146 deg s^{-1}, $N=122$), whereas for turns away, when translational and rotational flow are in the same direction, it is 161 deg s^{-1} (IQR: 84–305 deg s^{-1}, $N=173$). The relatively low image speed of the nest associated with pseudo-fixations during turns towards the nest is a consequence of the bee pivoting around the nest area and the bee's residual head rotation.

The wider pattern of image motion generated by these movements is shown in Fig. 4, which displays the absolute image speeds on the retina generated by a dense array of virtual features protruding above the ground plane at different distances from the nest. Each plot shows the flow field of one bee positioned ~5.5 cm from the nest-hole and flying at absolute directions ranging between 25 and 45 deg relative to the nest hole. The absolute image speed in all cases is high near the bee, where flow is dominated by the bee's translational movements.

The image speeds in the flow fields of the two bees turning towards the nest (Fig. 4A,C) drop towards the nest. The nest-hole is near to a circle of zero speed (the zero horopter) where translational and rotational flow cancel each other out, being equal in speed but in opposite directions. Outside the circle and beyond the nest the flow becomes increasingly dominated by rotation. The pattern of flow differs for the two bees turning away from the nest (Fig. 4B,D). In these cases, image speed close to the nest is relatively high, with translational and rotational flow in the same direction. The pattern of the bees' movements during turns towards the nest thus highlights visual features near the nest and potentially marks them as features to be remembered.

Signs of pivoting parallax detected in low speed recordings

The high resolution recordings view a limited region around the nest. To determine whether a pattern of flight consistent with pivoting parallax applies over a somewhat larger area when bees are up to 30 cm from the nest, we re-analysed the loops of learning flights recorded with two cylinders placed ~20 cm NNE and 20 cm SSW of the nest (Fig. 5A) (Philippides et al., 2013). The low spatial resolution of the recordings means that image movements of visual features over the retina are approximated by calculations from
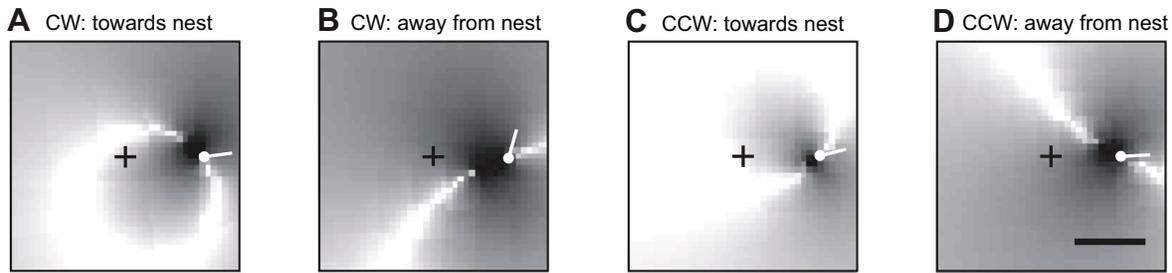
Fig. 4. Pivoting parallax during pseudo-fixations. Estimated image speed of visual features around the nest for four bees (white ball-and-stick) during a pseudo-fixation as the bees turn towards (A,C) and away from (B,D) the nest (+), either CW (A,B) or CCW (C,D). The data come from examples of bees positioned about 5.5 cm from the nest. To make the individual flow fields easier to compare, the bees' circumferential positions around the nest have all been rotated to three o'clock. The bees fly at an absolute direction relative to the nest, ranging between 25 and 45 deg. The orientations of their body relative to the nest are 8, 74, 15 and 3 deg for A–D, respectively. Image speeds are shown on a log scale (to avoid the loss of detail due to the high translational speed around the bee) as white (0) to black (maximum). Scale bar, 5 cm.

changes in body orientation and position. Fig. 5B shows (separately for clockwise and counter-clockwise loops) the angular speeds of the bee's body, of the nest and of the more northerly cylinder across the retina. Each of these parameters is plotted against the orientation of the bee's body relative to the nest.

The pattern of results resembles that seen with head movements (Fig. 3). But in terms of absolute speed, angular body speeds averaged across saccades and fixations are obviously higher than the angular speed of the head during pseudo-fixations. The first similarity between the two sets of results is that the bee's body rotates faster during turns towards than away from the nest. Second, the image of the nest moves more slowly across the retina during turns towards than away from the nest. Additionally, the image of the cylinder moves more rapidly than that of the nest during the
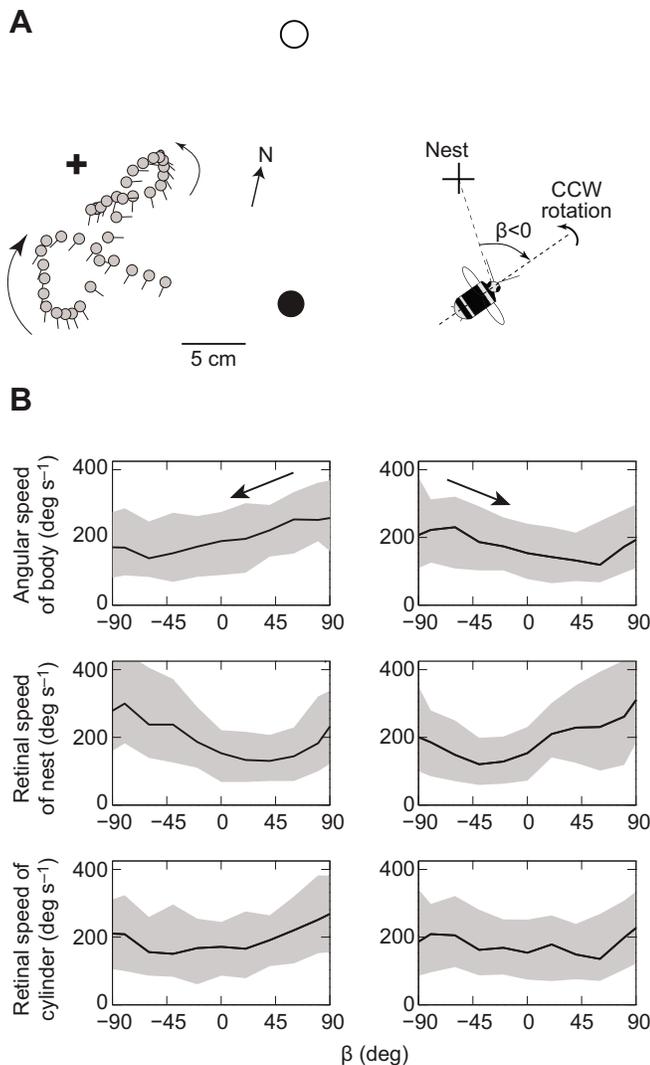

Fig. 5. Pivoting parallax during loops. (A) A pair of CW and CCW loops recorded at 50 frames s^{-1}. +, nest; the large black and white circles are 20 cm high cylinders. The cartoon on the right demonstrates the convention used for the variables. For CW rotations, β (body orientation relative to nest) is positive during turns to the nest. For CCW rotations, β is negative. (B) Top row: median angular speed of the body plotted against the angle of the body during 92 CW (left) and 93 CCW (right) loops over the range −90 to +90 deg. The shaded area is the IQR. Bins are 20 deg wide. The arrow denotes the direction of travel through the loop. Centre row: same data showing the median speed of the image of the nest across the retina and the IQR estimated from the orientation of the body. Bottom row: median speed and IQR of the more northerly cylinder (white circle) across the retina. Shaded areas indicate the IQR of the data. (C) Median angular speeds of the retinal image of different positions around the nest and landmarks for CW (upper two panels) and CCW (lower two panels) turns towards (first and third panels) and away from (second and fourth panels) the nest. Data are shown in greyscale from white (low, 120 deg s^{-1}) to black (high, 320 deg s^{-1}) from the same loops as in B. +, nest; the white and black circles indicate 20 cm high cylinders. Further details are given in Materials and methods.
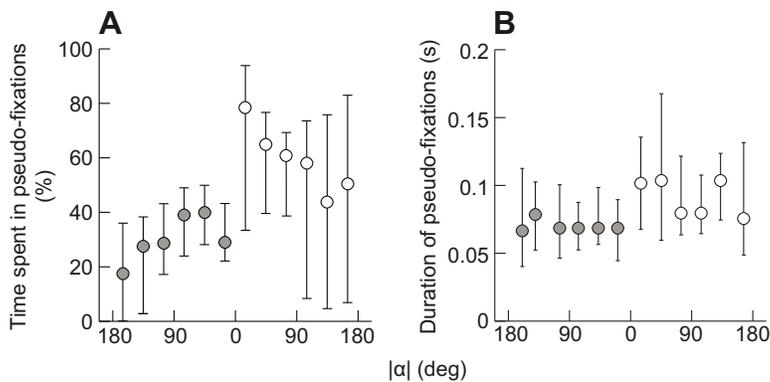
Fig. 6. Duration and percentage of time spent in pseudo-fixations. (A) The median percentage of total flight time spent in fixations plotted against the absolute orientation of the head relative to the nest (|α|). Open and filled circles correspond respectively to flight away from and towards the nest. Median percentages are calculated over 30 flights and over 30 deg bins of absolute head orientation relative to the nest. Error bars mark the 25th and 75th percentiles of the data. (B) Duration of pseudo-fixations plotted against absolute head orientation relative to the nest. Calculations and conventions as in A. Error bars mark the 25th and 75th percentiles of the data. Fixations last longer when the bee turns away from the nest.

relevant segment of loops towards the nest, even though bumblebees tend to approach the nest from a direction that places the bee closer to the nest than to the cylinder (Philippides et al., 2013).

Fig. 5C displays the spatial distribution of the median image speeds of a dense array of features close to the ground when the bee turns towards the nest over the range of body orientations ±45 to ±15 deg relative the nest. Speeds are then low around the nest and increase with distance from it. The inverse distribution is found during turns away from the nest over the same range of body orientations relative to the nest. The data in Fig. 5B,C are thus consistent with the use of pivoting parallax during turns towards the nest, but not during turns away from the nest.

DISCUSSION

Insects, which have their eyes positioned close together, generally rely on motion parallax for 3D scene analysis and often eliminate rotational optic flow (reviewed in Egelhaaf et al., 2012). Rotational optic flow carries little useful information about the structure of the world when the rotating observer is positioned at the centre of rotation and sees the images of objects at all distances rotating at the same speed. The situation changes when the observer rotates about a point some distance away (Zeil, 1993a); in this case the apparent speed of objects depends on their position relative to the observer and to the centre of rotation. As Zeil suggested (Zeil, 1993a), and as we outlined in the Introduction, the information generated by such pivoting parallax would be particularly helpful to an insect learning about the immediate surroundings of its nest and needing to assess which salient visual features lie near to the nest.

We have described how the coordinated head and body movements of bumblebees make particular phases of learning flights well-suited to gauging the proximity of visual features to the nest through pivoting parallax. Bees do not move their heads enough to reduce rotational image speed completely during pseudo-fixations. This under-compensation of head-on-body movements, on which the bumblebee's pivoting parallax relies, is found throughout a learning flight. It occurs during turns towards and away from the nest (Fig. 3C), and also in parts of the flight in which the trajectory has no clear pattern (supplementary material Fig. S1C,D). But the under-compensation helps generate potentially useful visual feedback only during pseudo-fixations in which bees turn towards the nest with relatively high rotational speeds of the head and body (Fig. 3A,B).

The opposing directions of rotational and translational optic flow on the nest side during pseudo-fixations in turns towards the nest mean that the nest-hole and visual features close to it move relatively slowly across the retina (Fig. 3D), implementing a form of pivoting parallax (Fig. 4 and Fig. 5C). During the course of a learning flight, flight manoeuvres extend over a progressively larger area and the bee's translational speed increases proportionally to its distance from the nest with little change in rotational speed (Philippides et al., 2013), as also happens in *Cerceris* (Zeil, 1993a). We can thus expect the flow-field pattern of Fig. 4 and Fig. 5C to enlarge as the bee's loops take it further from the nest.

If bees were to pivot precisely about the nest-hole, then the minimum image speed would be located coincidently with the nest-hole (Fig. 4 and Fig. 5C). The lack of precise coincidence suggests that the major benefits of the bumblebee's strategy may be to reduce the image speeds of visual features close to the nest, thereby enhancing their visibility through motion contrast and signalling their proximity to the nest rather than giving precise distance information.

This pivoting pattern of optic flow occurs during loops just before the brief period when bees face the nest (Fig. 5). It is difficult to learn much about the duration of nest-facing from recordings that are too slow to separate saccades and pseudo-fixations. High speed recordings reveal that the durations and frequencies of pseudo-fixations are greatest around and just after nest facing (Fig. 6). This timing is intriguing. It adds support to the suggestion that wasps and bees may store the retinal positions of features when facing the nest and guide their return trips to the nest using this stored information (Collett, 1995). Bumblebees might thus highlight through pivoting parallax which visual features are to be emphasised in their stored views, just before committing those views to memory. Interestingly, there are close similarities between the bees' manoeuvres in both learning and return flights before, during and just after nest-facing (Philippides et al., 2013), so that similar parallax information and views of the nest are available to returning and to departing bees.

MATERIALS AND METHODS
Recordings

Two sets of recordings were made of the learning flights of *B. terrestris*. Dataset A was made using foragers from a single colony on the flat roof of a four-storey building at the University of Exeter, Exeter, UK. The nest box holding the colony was placed under a 150×150 cm table. A plastic tube connected the nest box to a ca. 1 cm exit hole in the centre of the table aligned with a hole in a white bath mat which covered the table top. During all recordings, an upright, black cylinder (8 cm high, 2.6 cm in diameter) was positioned 8 cm to the north of the exit hole. Manually operated doors controlled the passage of bees so that single bees could leave the nest and their flights be recorded without interference. Eighteen foragers were marked with number plates on their thorax and dabs of paint on their abdomen. The bees' first and subsequent departure flights were recorded with a Phantom V5.1 digital high-speed video camera. The camera was suspended 1.3 m above the table top. It was supported by a metal cross attached to four vertical struts, one at each corner of the table. The diagonals of the table top were aligned north–south and east–west. The camera viewed a 20×20 cm area that was centred on the nest-hole. Monochrome video

recordings were made at 250 frames s^{-1} with a frame resolution of 1024×1024 pixels. The maximum duration of a recorded flight was 15 s. Source video files were saved on a hard drive in uncompressed AVI format for later offline processing in MATLAB (The MathWorks, Inc.) using custom-written software.

The second set of recordings, dataset B, used a similar set-up in the grounds of the University of Exeter. The spatial and temporal (500 frames s^{-1}) resolution of the recordings were higher in order to detect and follow the movement of two or more spots of white paint that were applied to the top of the bees' heads (Fig. A1A). As in dataset A, most of the recordings were from above. We also recorded some flights with the camera oriented horizontally and pointing in the direction of the nest entrance. For a short period we were able to record flights with two cameras, one looking down and the other sideways. Data for Fig. 5 were recorded as described in Philippides et al. (Philippides et al., 2013).

Analysis of data from dataset A
The orientation of the bee's head and body and their positions in the horizontal plane were extracted from each frame of a recorded flight. For most of the reported data, head orientation was obtained by modifying a method used previously (Boeddeker et al., 2010). For each frame, an enlarged picture of the head and part of the thorax was rotated until the outline of the head and antennae was judged to face directly upwards. To be sure that the measurements of successive frames were unbiased, a random rotation uniformly distributed in the range −10 to +10 deg was added to the orientation of each frame and then subtracted after the orientation of the frame had been adjusted. The orientation of the bee's longitudinal body axis was also obtained using custom-written MATLAB software, which fitted an ellipse to the image of the bee. Horizontal position (x- and y-coordinates) was calculated as the centre of mass of the image. Both orientation and position were corrected by hand if necessary. In total, 13 learning flights (24,237 frames) from nine bumblebees were analysed with this method.

Custom-written MATLAB software categorised the bees' rotational movements into saccades and pseudo-fixations according to the speed of head rotation. Saccades were extracted automatically as peaks in the time plot of the smoothed angular speed of the head, plus connected sets of those data points around the peak that were above a set threshold of 375 deg s^{-1}. Pseudo-fixations were also extracted automatically as continuous fragments between two saccades with a smoothed rotational speed of less than 100 deg s^{-1} at each point of the fragment. The beginning and ends of saccades and fixations are sufficiently abrupt (Fig. 1B) to time them within about 4 ms (one video frame).

Long fragments of flight that corresponded to staircases of CW or CCW rotations were extracted by eye from plots of head and body orientation over time. Typically, there were four to five of these fragments in each recorded flight. These fragments were divided manually into head turns towards or away from the nest. There were on average nine of each of these turn segments in each flight. Flight direction was determined from a line fitted to the bee's x–y coordinates over neighbouring frames and translational speed from the Cartesian distance between neighbouring frames.

Of the total flight time, 55% was categorised automatically as either a fixation or a saccade. The remaining 45% consisted of the transitions between CW and CCW turning (24%, supplementary material Fig. S1D) and of portions of flight that were too noisy for the program to categorise.

The data in Fig. 6, which only require measurement of the duration of a pseudo-fixation, used a different method to determine head orientation. The base of each antenna was marked manually on each frame. Head direction was taken as the perpendicular to the line connecting the two marks. Fixations and saccades were then selected manually from the plot of head orientation over time. We had initially analysed 30 flights (59,885 frames) with this method, before re-analysing a subset of 13 of these flights with the modified Boedekker method to obtain measurements that might be less prone to noise. All calculations and illustrations in the main text, with the exception of Fig. 6, relied entirely on flights in which head orientation was obtained using the Boedekker method. To maximise the number of fixations included in Fig. 6, we used data from all 30 flights.

We measured various characteristics of each saccade and pseudo-fixation, such as their speed and orientation. For description and for statistical comparisons, we calculated the median and IQR of speed, orientation, etc., for distributions of fixations and saccades. The statistical significance of differences between distributions was then assessed using the non-parametric Kolmogorov–Smirnov test. The significance of differences between the medians of distributions, or between the median value of a distribution and zero, were assessed with the Wilcoxon rank sum test. The centre of the nest-hole was used to define the nest's position on the retina.

Computation of image motion across areas near the nest
Figs 4 and 5 illustrate the instantaneous retinal speeds of a dense array of stationary visual features in a horizontal area around the nest, which are assumed to be in the same horizontal plane as the bee. Retinal image speeds in Fig. 4 are estimated from the instantaneous movements of four bees during pseudo-fixations, assuming that the rotational and translational velocities of the bees, measured at the centre of the pseudo-fixation, are constant for 89 ms (the median length of a pseudo-fixation). Retinal image speeds in Fig. 5 (including the retinal speed of the nest and cylinders) are calculated from bees performing 92 CW and 93 CCW loops extracted from video recordings at 50 half-frames s^{-1} (Philippides et al., 2013). For each time point in the loop, the rate of change of the retinal image of each feature on the retina is calculated from neighbouring time points via the 'gradient' function in MATLAB. For Fig. 5C, data are collated from small sections of the loops in which the bee turns towards or away from the nest and in which the nest lies within the bee's fronto-lateral visual field. For CW loops, data are restricted to sections where the orientation of the bee's body relative to the nest (β in Fig. 5A) is in the range 15–45 deg for turns towards the nest and –45 to −15 deg for turns away from the nest. For CCW loops, the direction is reversed (β is –45 to −15 deg for turns towards and 15 to 45 deg for turns away from the nest). We then calculate the median retinal speed (absolute value of the rate of change) of each feature across turns towards and away from the nest in each loop.

APPENDIX
Analysis of dataset B to determine head roll during pseudo-fixations and to estimate possible errors in measurements of head yaw
Analysis methods
Head orientation was extracted by tracking manually the positions of two obvious features (a white paint mark on a bee's head) between all frames of a flight (Fig. A1A, points A and B). To avoid any possibility of including transitions between saccades and pseudo-fixations, we excluded the beginning 10% and end 10% of each pseudo-fixation. To examine interactions between yaw and roll, we selected a third conspicuous point on the bee's head (Fig. A1A, point C) so that the three points formed a clear triangle and the third point was close to the anterior–posterior axis (Fig. A1A, white dashed line). Next, we calculated the angular speeds in a horizontal plane of the three lines (AB, AC, BC) of the triangle. We also selected two points that lie on the midline of the head in order to calculate the angular speed of the midline.

Estimating head roll
Because head angular speeds during pseudo-fixations when measured by monitoring spots (dataset B) are similar to the data from dataset A, analysed with the Boedekker method (Fig. A2, top row, Wilcoxon rank sum test, $P>0.3$), we have analysed dataset B for information about the possible contribution of roll to yaw and we assume that the conclusions apply to both datasets.

To assess the contribution of roll, we assumed that both roll and yaw are present, and modelled the bee's head as a cylinder (Fig. A1B). In this model, the three points lie on the surface of a cylinder, the long axis of which is the roll axis (Fig. A1B, line rr). The apparent angular speed of each of the lines may then be represented as $\omega=\omega_{yaw}+k\sin(2\beta)$, where ω_{yaw} is the yaw component
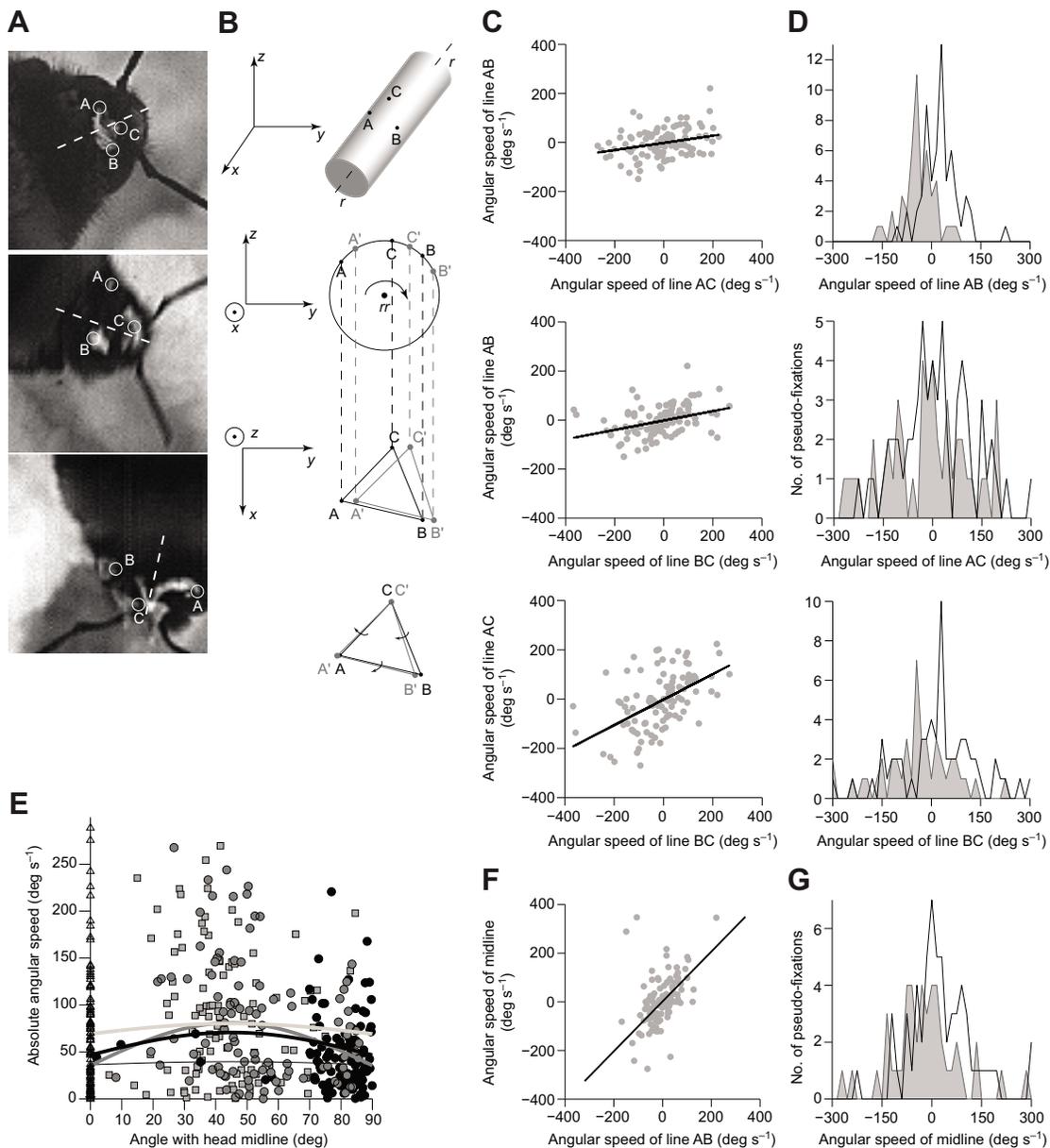
Fig. A1. Assessing the contribution of head roll to measurements of yaw (dataset B). (A) Examples of white paint marks on bees' heads. Circles A, B and C mark the positions of the points, the coordinates of which were extracted and used to estimate the speed of head rotation. The dashed line marks the position of the head midline. (B) Cylindrical model of a bee's head during a period of roll. A, B and C correspond to the three points marked on the bee's head (as in panel A). The dashed *rr* line indicates the roll axis. From the top, the first panel shows the relative 3D orientation of the marked points and roll axis for a typical example. The second panel demonstrates how the marked points move during a CW roll, viewed in the *y–z* plane. A′, B′ and C′ indicate the positions of the marked points at the end of the turn. The third panel shows the same CW roll in the *x–y* plane – the plane that is visible in our video recordings (compare with panel A). The fourth panel shows the same triangles as in the third panel, with C and C′ superimposed. Arrows indicate the direction of rotation of the three lines AB, AC and BC, and show that roll without yaw can generate the same direction of rotation for all three lines. (C) Correlation between angular speeds of the three lines. Data are from 105 pseudo-fixations (14 learning flights), selected so that the length of each of the three lines is always greater than 5 pixels. The correlation coefficient for AB and AC (top) equals 0.32, for AB and BC (middle) it is 0.36, and for AC and BC (bottom) it is 0.5. (D) Angular speeds of the three lines, separated into CW (grey lines, shaded) and CCW (black lines) rotations (compare with Fig. A2). (E) Absolute angular speed of lines AB (black circles, thin black line), BC (dark grey circles, thick dark grey line) and AC (light grey squares, thick light grey line) plotted against the angle β that the corresponding line makes with the head midline (dashed line in panel A). Grey and thin black lines are the fits to the data [*a*+*b*×sin(2×β)], calculated for each of the three lines separately, and black solid line shows the fit to all datapoints together (*a*=46.5, *b*=24). Triangles denote speeds of the midline. (F) Correlation between angular speed of the midline and the roughly perpendicular line AB. (G) Angular speed of the midline separated into CW and CCW rotations, as in panel D.

and $k\sin(2\beta)$ is the roll component. The coefficient k depends on the exact positions of A, B or C relative to each other and the head midline. β is the angle that AB, BC or AC forms with the head midline (β=0 for the head midline).

Yaw will cause all three sides of the triangle to rotate with the same angular speed in the same direction. The potential effect of roll is more complex. Lines AC and BC are most likely to rotate in the same direction, while AB may rotate either CW or CCW, depending
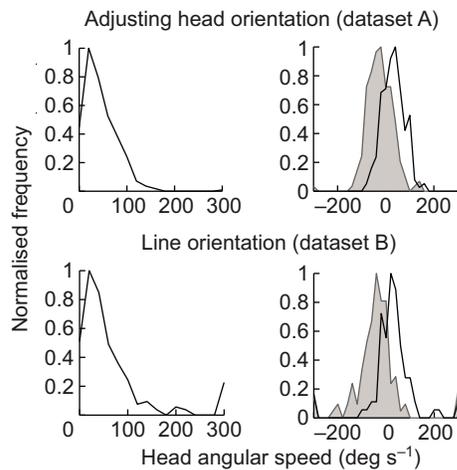
Fig. A2. Comparison of angular head speeds during pseudo-fixations from datasets A and B. Left column shows distributions of the absolute value of head speed from two separate data sets with head orientation measured in two different ways (as described in the Appendix). Right column shows the same data, plotted according to the direction of rotation, being CCW (blackline, positive direction) or CW (grey line, shaded, negative direction). Data in the top row are re-plotted from Fig. 2A.

on the relative positions of A and B along the *y*-axis. An example of all three lines, AC, BC and AB, rotating in the same direction is illustrated in Fig. A1B. Roll will affect lines AC and BC much more than line AB, because AB forms a larger angle with the head axis, and should not affect the head axis at all.

Were yaw to dominate, this model predicts that the angular speeds of the three lines would be highly correlated. In the presence of roll, the speed of lines AC and BC should be higher than that of AB. The speed of AC and BC should be positively correlated, and this correlation should be stronger than for AC/AB and BC/AB pairs. According to this model, the actual data (Fig. A1C) imply that there is a roll component present, as the speeds of AC and BC are positively correlated, and both are larger than that of AB. Nonetheless, these relationships are inadequate to decide whether roll is the principal cause of the CW/CCW angular speed difference seen in Fig. 2A.

To tease apart the contributions of roll and yaw, we note that the effect of roll is weakest for the AB line, and much stronger for lines AC and BC. Thus, if the CW/CCW difference in angular speed is caused primarily by roll, the average speed of the AC and BC lines should differ from zero more than the speed of AB. Fig. A1D shows the angular speeds of the three lines, plotted according to CW (grey line, negative direction) or CCW (solid line, positive direction) rotation of the flanking saccades. The distance from 0 of the median values for CW and CCW rotations is comparable for lines AB (CCW: 23.3 deg s^{-1}, IQR: −10.2 to 57.1 deg s^{-1}; CW: −43.2 deg s^{-1}, IQR: −60.7 to −11 deg s^{-1}) and BC (CCW: 25.7 deg s^{-1}, IQR: −32.5 to 94.7 deg s^{-1}; CW: −42.7 deg s^{-1}, IQR: −106.1 to 24.8 deg s^{-1}), and is smaller for line AC (CCW: 7.4 deg s^{-1}, IQR: −53.3 to 90.7 deg s^{-1}; CW: −8.4 deg s^{-1}, IQR: −105.6 to 68 deg s^{-1}), indicating that yaw, and not roll, rotations are the cause of the separation.

To assess the magnitude of the roll component $k\sin(2\beta)$, we have plotted the absolute angular speed of AB, BC and AC (and the speeds of the head midline) against the angle β that these lines form with the head midline (Fig. A1E); the black solid line depicts the function $\omega_{yaw}+k\sin(2\beta)$, fitted to all data points shown on the figure

(MATLAB *cftool* function, NonLinearLeastSquares method with LAR robust minimization and Trust-Region algorithm). The fit coefficients obtained were ω_{yaw}=46.5, k=24, indicating that, for the line AB (β=70–90 deg), the relative contribution of roll may be up to 30%. Nonetheless, because the biggest difference between CW and CCW speeds across pairs of lines is not between AC and BC, the roll component cannot explain the directionality of residual head rotations during pseudo-fixations.

This conclusion is supported by two additional results. First, the speeds of the midline and line AB are correlated (Fig. A1F), even though there is ca. 90 deg difference between their orientations. As the speeds of both lines should have very small contributions from roll, the correlation will be mostly due to yaw. Also, like the line AB, the median angular speeds of the midline during CW and CCW pseudo-fixations differ significantly (CCW: 12.9 deg s^{-1}, IQR: −22 deg s^{-1} to 84 deg s^{-1}; CW: −24.6 deg s^{-1}, IQR: −73 deg s^{-1} to 22.6 deg s^{-1}, P=0.0077).

Second, the duration of yaw turns in one direction in these recorded flights is approximately 1 s (median: 1.05 s, IQR: 0.9–1.4 s, N=18), while the duration of a bout of roll in one direction is much shorter. Roll was analysed from high speed video recordings taken with the camera viewing the scene from the side. The direction of roll could be determined when the bee was roughly facing the camera. A bout of roll in one direction lasted about 120 ms (median: 122 ms, IQR: 98–190 ms, N=30) and was often followed by a bout in the opposite direction. Occasional examples were obtained with the bee visible from the top and the side. Yaw and roll were to the same side in seven cases and to opposite sides in six cases. The reasons for the rapid changes in the direction of roll are not clear. One possibility is that the low flying bees are reacting to the rough surface of the bath mat over which they travel. In any case, these differences between yaw and roll indicate that the direction of roll and yaw are not strongly correlated.

Data are available by request to oriabinina@gmail.com.

References
Becker, L. (1958). Untersuchungen über das heimfindevermögen der bienen. *Z. Vgl. Physiol.* **41**, 1-25.
Bender, J. A. and Dickinson, M. H. (2006). Visual stimulation of saccades in magnetically tethered *Drosophila*. *J. Exp. Biol.* **209**, 3170-3182.
Blaj, G. and van Hateren, J. H. (2004). Saccadic head and thorax movements in freely walking blowflies. *J. Comp. Physiol. A* **190**, 861-868.
Boeddeker, N., Dittmar, L., Stürzl, W. and Egelhaaf, M. (2010). The fine structure of honeybee head and body yaw movements in a homing task. *Proc. Biol. Sci.* **277**, 1899-1906.

Brünnert, U., Kelber, A. and Zeil, J. (1994). Ground-nesting bees determine the location of their nest relative to a landmark by other than angular size cues. *J. Comp. Physiol. A* **175**, 363-369.

Capaldi, E. A. and Dyer, F. C. (1999). The role of orientation flights on homing performance in honeybees. *J. Exp. Biol.* **202**, 1655-1666.

Cheng, K., Collett, T. S., Pickhard, A. and Wehner, R. (1987). The use of visual landmarks by honeybees: bees weight landmarks according to their distance from the goal. *J. Comp. Physiol. A* **161**, 469-475.

Collett, T. S. (1978). Peering – a locust behaviour pattern for obtaining motion parallax information. *J. Exp. Biol.* **76**, 237-241.

Collett, T. S. (1995). Making learning easy: the acquisition of visual information during the orientation flights of social wasps. *J. Comp. Physiol. A* **177**, 737-747.

Collett, T. S., de Ibarra, N. H., Riabinina, O. and Philippides, A. (2013). Coordinating compass-based and nest-based flight directions during bumblebee learning and return flights. *J. Exp. Biol.* **216**, 1105-1113.

Dittmar, L., Egelhaaf, M., Stürzl, W. and Boeddeker, N. (2011). The behavioural relevance of landmark texture for honeybee homing. *Front. Neural Circuits* **5**, 20.

Egelhaaf, M., Böddeker, N., Kern, R., Kurtz, R. and Lindemann, J. P. (2012). Spatial vision in insects is facilitated by shaping the dynamics of visual input through behavioural action. *Front. Neural Circuits* **6**, 108.

Land, M. F. (1973). Head movement of flies during visually guided flight. *Nature* **243**, 299-300.

Land, M. F. (1997). Visual acuity in insects. *Annu. Rev. Entomol.* **42**, 147-177.

Lehrer, M. (1993). Why do bees turn back and look? *J. Comp. Physiol. A* **172**, 549-563.

Lehrer, M. and Collett, T. S. (1994). Approaching and departing bees learn different cues to the distance of a landmark. *J. Comp. Physiol. A* **175**, 171-177.

Opfinger, E. (1931). Über die orientierung der biene an der futterquelle. *Z. Vgl. Physiol.* **15**, 431-487.

Osborne, J. L., Smith, A., Clark, S. J., Reynolds, D. R., Barron, M. C., Lim, K. S. and Reynolds, A. M. (2013). The ontogeny of bumblebee flight trajectories: from naïve explorers to experienced foragers. *PLoS ONE* **8**, e78681.

Philippides, A., de Ibarra, N. H., Riabinina, O. and Collett, T. S. (2013). Bumblebee calligraphy: the design and control of flight motifs in the learning and return flights of *Bombus terrestris*. *J. Exp. Biol.* **216**, 1093-1104.

Ribak, G., Egge, A. R. and Swallow, J. G. (2009). Saccadic head rotations during walking in the stalk-eyed fly (*Cyrtodiopsis dalmanni*). *Proc. Biol. Sci.* **276**, 1643-1649.

Schilstra, C. and van Hateren, J. H. (1999). Blowfly flight and optic flow. I. Thorax kinematics and flight dynamics. *J. Exp. Biol.* **202**, 1481-1490.

Schilstra, C. and van Hateren, J. H. (1998). Stabilizing gaze in flying blowflies. *Nature* **395**, 654-654.

Sobel, E. C. (1990). The locust's use of motion parallax to measure distance. *J. Comp. Physiol. A* **167**, 579-588.

Tinbergen, N. (1932). Über die orientierung des bienenwolfes (*Philanthus triangulum* Fabr.). *Z. Vgl. Physiol.* **16**, 305-335.

van Hateren, J. H. and Schilstra, C. (1999). Blowfly flight and optic flow. II. Head movements during flight. *J. Exp. Biol.* **202**, 1491-1500.

Vollbehr, J. (1975). Zur orientierung junger honigbienen bei ihrem orientierungsflug. *Zool. Jb Allg Zool. Physiol.* **79**, 33-69.

Voss, R. and Zeil, J. (1998). Active vision in insects: an analysis of object-directed zig-zag flights in wasps (*Odynerus spinipes*, Eumenidae). *J. Comp. Physiol. A* **182**, 377-387.

Wagner, W. (1907). Psychobiologische untersuchungen an hummeln. *Zoologica* **46**, 1-238.

Wallace, G. K. (1959). Visual scanning in the desert locust *Schistocerca gregaria* Forskål. *J. Exp. Biol.* **36**, 512-525.

Zeil, J. (1993a). Orientation flights of solitary wasps (*Cerceris*; Sphecidae; Hymenoptera) I. Description of flights. *J. Comp. Physiol. A* **172**, 189-205.

Zeil, J. (1993b). Orientation flights of solitary wasps (*Cerceris*; Sphecidae; Hymenoptera) II. Similarities between orientation and return flights and the use of motion parallax. *J. Comp. Physiol. A* **172**, 207-222.

Zeil, J., Boeddeker, N., Hemmi, J. M. and Stürzl, W. (2007). Going wild: toward an ecology of visual information processing. In *Invertebrate Neurobiology* (ed. G. North and R. J. Greenspan), pp. 381-404. Cold Spring Harbor, NY: Cold Spring Harbor Laboratory Press.